Design of a Two Degree of Freedom Resonant Miniature Robotic Leg

Shannon A. Rios[1], Andrew J. Fleming[2] and Yuen Kuan Yong[3]

***Abstract*— This article identifies the design considerations for a two degree of freedom (DoF) miniature robotic leg utilizing piezoelectric bimorph actuators with a specific focus on the resonance modes of the system. An analytical model was developed using three independent lumped mass models with superposition for tuning the resonance frequencies and optimizing the performance of the leg. The model was verified both experimentally and using FEA.**

I. Introduction

There are many advantages to the miniaturization of autonomous robots. The reduction in size allows the robot access to restricted locations such as, inside water pipes [1], through rubble [2], [3] and even inside the human body [4]. Another advantage is the potential reduction in cost and the possibility for disposable robots. Additionally, due to the small power requirements, it is possible to power a miniature robot from ambient energy sources such as light, electric fields, magnetic fields or vibration [5].

There are several challenges associated with designing a miniature robot. The reduced size of the robot increases the complexity of the power supply, mechanical design, sensors and control of the robot. To combat this, aspects of the design are simplified to reduce the complexity. One common method of reducing the complexity is to reduce the number of actuators or degrees of freedom (DoF) the robot has.

There has been an increased interest in the development of miniature robots over the past decade [6]. For example, Wood et al have developed several miniature robots utilizing piezoelectric bender actuators for locomotion [7]–[11]. One such example is a 1.7 g hexapod configuration autonomous robot that was able to achieve a forward travel speed of 0.9 body lengths per second [12]. This robot was approximately 4.8 cm long and consisted of three leg pairs where each pair of legs were driven by three piezoelectric benders arranged to amplify the displacement and produce a tripod gait.

The use of resonant vibration in miniature robotics was reported in [13]. Their work outlines the development of a range of robots capable of traveling over both land and water. These robots used forced vibration of continua to achieve two axis locomotion utilizing a single piezoelectric actuator. This actuator was driven with frequencies between 0.1 to 100 kHz.

This article investigates the design of a two DoF miniature robot leg. In order to generate locomotion two piezoelectric benders are used. The displacement of the benders are amplified by the mechanical structure of the leg and by driving the two benders at the resonances of the system, a high speed gait can be achieved. The main focus of this work is to identify key design parameters and insights that dictate the resonant frequencies of the miniature robot leg and their associated motion. To achieve this, three lumped mass models are derived and combined using superposition. The model is then compared to FEA and real world experimental results.

The following section will outline the overall leg design, including the physical layout and electrical configuration. Next the parameters for the lumped mass model of the leg are derived and compared to experimental results. The paper will be concluded with a discussion on the key parameters effecting the resonant frequencies of the leg and an outline of the future direction.

II. Leg configuration

The size and shape of the leg is intended to be used on a hexapod style miniature robot similar in design to the one shown in Fig. 1. Each leg consists of two parallel piezoelectric bimorph benders joined at the tip by an aluminum end-effector comprised of a flexure part and a leg part as shown in Fig. 2. Unlike most other miniature robot legs [14], the piezoelectric actuators are integrated into the mechanical structure.

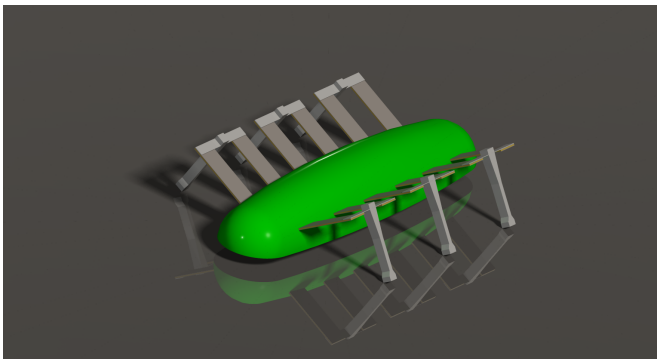

Fig. 1. 3-D representation of a hexapod robot using this leg design

The benders are driven using the biased bipolar electrical configuration [15] which utilizes both the positive and negative electric fields for maximum deflection and force.

The authors are with the Precision Mechatronics Laboratory, School of Electrical Engineering and Computer Science at the University of Newcastle, Callaghan, NSW 2308, AUSTRALIA

[1]Shannon.Rios@newcastle.edu.au

[2]Andrew.Fleming@newcastle.edu.au

[3]Yuenkuan.Yong@newcastle.edu.au

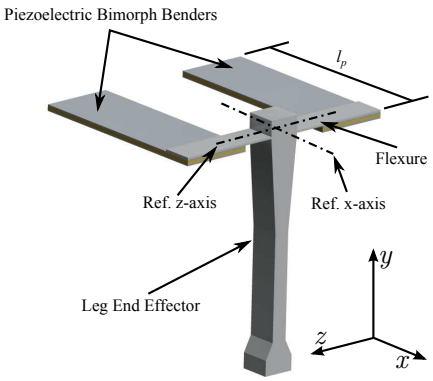

Fig. 2. Prototype two degree of freedom piezoelectric leg

By driving each bender with a sinusoidal waveform and varying the phase between the two benders a wide range of end effector motion paths can be achieved. Of most interest, when driven 90° out of phase a circular motion at the tip of the end effector can be produced. A miniature robot comprised of several legs can be controlled by varying the phase and magnitude of each leg.

The unique design of the leg results in two resonant modes that are reasonably close together and by altering a small set of variables these resonant modes can be made to overlap. In general the first resonant mode is dominated by rotation about the z-axis and is referred to as the lifting mode. The second resonant mode is characterized by rotation about the x-axis and is referred to as the swinging mode. By forcing these modes to overlap the resonant motion of the leg will be a combination of lifting and swinging.

III. Modeling

The modal superposition technique is used to develop a 3-DoF lumped mass model for the previously discussed miniature robot leg. This method was chosen over numerical methods as a lumped mass model can be used to provide insight into the design parameters of the system. This technique uses superposition of multiple single DoF lumped mass systems to create a complete model of the system. Each individual system is comprised of either a mass, stiffness and force, or a torque, rotational stiffness and rotational inertia as per Fig. 3, where M is the mass, I is the rotational inertia, K is the stiffness, F is the force and τ is the torque.

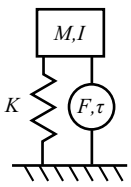

Fig. 3. Single DoF equivalent lumped mass model

Each lumped mass system will be related to a point that is along the centroid of the flexure and midway between the two piezoelectric benders, shown in Fig. 2. The three axis to be determined are: displacement along the y-axis δ_y, rotation about the x-axis θ_x and rotation about the z-axis θ_z. In order to solve the dynamic equation and find the resonant frequencies, the stiffnesses, mass and inertias of the individual systems must be determined. The damping factor of the system is ignored to simplify this analysis.

A. Linear DoF δ_y

The resonant frequency for a single DoF system is given by $f = \frac{1}{2\pi}\sqrt{\frac{K}{M}}$. In order to determine the stiffness and mass parameters for the y-axis an appropriate model for the system must be developed. Fig. 4 shows the mass and stiffness model used for the y-axis lumped mass model. This model was used in combination with the Rayleigh method of equating the maximum potential energy to the maximum kinetic energy of the system, $PE_{\max} = KE_{\max}$. In order to solve this equation the relative displacements and velocity of each mass were found, assuming sinusoidal motion, such that,

$$\delta_y = \delta_{\max}, \tag{1}$$

$$\delta_p = \delta_{\max} A, \tag{2}$$

$$v_y = \dot{\delta}_y \tag{3}$$

$$= \omega \delta_{max}, \tag{4}$$

$$v_p = \omega \delta_{max} A, \tag{5}$$

$$A = \frac{K_f}{K_f + K_p}, \tag{6}$$

where δ_y is the displacement of the leg mass, $\delta_{\max}$ is the maximum displacement, δ_p is the displacement of the bender mass, v_y is the velocity of the leg mass, V_p is the velocity of the bender mass, ω is the rotational velocity and K_p and K_f are the stiffnesses of the bender and flexure.

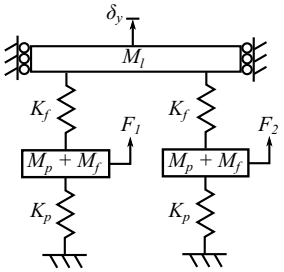

Fig. 4. Lumped mass model for y-axis DoF.

Using Eq. (1) to (6) and by analyzing half of the model due to symmetry, the maximum potential energy of the system is,

$$PE_{\max} = \frac{1}{2}\left[K_f(\delta_{\max} - \delta_{\max} A)^2 + K_p(\delta_{\max} A)^2\right], \tag{7}$$

$$= \frac{1}{2}\delta_{\max}^2\left[K_f(1-A)^2 + K_p A^2\right]. \tag{8}$$

Similarly the maximum kinetic energy is given by,

$$KE_{\max} = \frac{1}{2}\left[(M_p + M_f)\omega^2\delta_{\max}^2 A^2 + \frac{M_l}{2}\omega^2\delta_{\max}^2\right], \quad (9)$$

$$= \frac{1}{2}\omega^2\delta_{\max}^2\left[(M_p + M_f)A^2 + \frac{M_l}{2}\right], \quad (10)$$

where M_y, M_p, M_l and M_f respectively are the lumped masses of the y-axis DoF, bender, leg and flexure respectively. Lastly, the lumped mass and stiffness can be found by equating the maximum potential and kinetic energy such that,

$$\omega = \sqrt{\frac{K_f}{(M_p + M_f)A^2 + \frac{M_l}{2}}}, \quad (11)$$

$$K_y = K_f, \quad (12)$$

$$M_y = (M_p + M_f)A^2 + \frac{M_l}{2}, \quad (13)$$

where M_y is the equivalent mass and K_y is the equivalent stiffness of the y-axis model.

The stiffness of the piezoelectric bender, K_p, with respect to the y-axis is found using the boundary conditions for a cantilever beam [16],

$$K_p = \frac{3Dw_p}{2l_p^3}, \quad (14)$$

where K_p is the stiffness of the beam, w_p is the width of the beam, l_p is the length of the beam and D is the flexural stiffness of a triple layer beam, given by $D = \int E(y)y^2\,\mathrm{d}y$ [15]. Similarly, the bending stiffness of the flexure is

$$K_f = \frac{36E_f I_f}{P^3}, \quad (15)$$

where K_f is the stiffness of the flexure, E_f is the Young's modulus of the flexure, I_f is the second moment of area of the flexure and P is the distance between the piezoelectric actuators.

The lumped mass, M_p, of the actuator was determined by looking at the kinetic energy of an element of the actuator, $dT = \frac{1}{2}m(x)v(x)^2$ and using a velocity of $v(x) = v_{max}\frac{x}{l_p}$ and the mass per unit length of $m(x) = \rho_p w_p t_p\,\mathrm{d}x$ where v_{max} is the velocity at the tip of the actuator, l_p is the free length of the actuator, ρ_p is the density, w_p is the width and t_p is the thickness of the actuator. By substituting the velocity and mass equations,

$$M_p = m_p\frac{1}{3}, \quad (16)$$

where $m_p = \rho_p w_p t_p l_p$. Similarly, the mass of the flexure attached to the actuator is

$$M_f = m_f\frac{w_p}{l_f}, \quad (17)$$

where $m_f = \rho_f w_f t_f l_f$, w_f is the width of the flexure, t_f is the thickness of the flexure and l_f is the length of the flexure. The mass of the free section of the flexure is ignored and the leg mass. The mass of the leg, $M_l = \int \rho_l A_l(y) l_l\,\mathrm{d}y$, is assumed to be completely lumped at the intersection of the reference x and z axis shown in Fig. 2.

B. Rotational DoF θ_x

The resonance frequency for a rotational model is given by or $f = \frac{1}{2\pi}\sqrt{\frac{K}{I}}$. The lumped mass model for the rotational DoF about the x-axis is shown in Fig. 5. The reference axis for this degree of freedom is located through the centroid of the flexure with respect to the y-z plane. Using this model the lumped parameters are,

$$K_{\theta x} = K_{fx} + 2K_p\left(\frac{P}{2}\right)^2, \quad (18)$$

$$I_x = 2I_{px} + I_{fx} + I_l, \quad (19)$$

where $K_{\theta x}$ and K_{fx} are the equivalent rotational stiffness for the x-axis DoF and the flexure respectively, I_x, I_{px}, I_{fx} and I_l are the rotational inertias of the equivalent system, actuator, flexure and leg respectively.

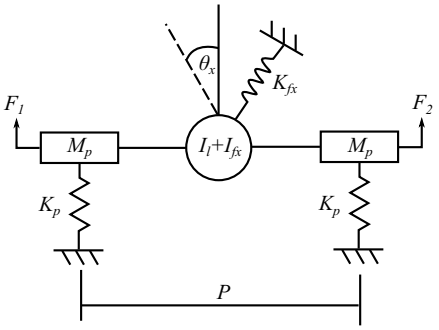

Fig. 5. Lumped mass model for θ_x DoF

Because of the symmetrical construction of the leg, the rotational stiffness K_{fx} was found by analyzing half of the flexure and assuming a guided - simply supported beam boundary condition [16], shown in Fig. 6. The angular displacement was found at the simply supported end and Hooke's law was used to determine the rotational stiffness,

$$K_{fx} = \frac{9E_f I_f}{P}. \quad (20)$$

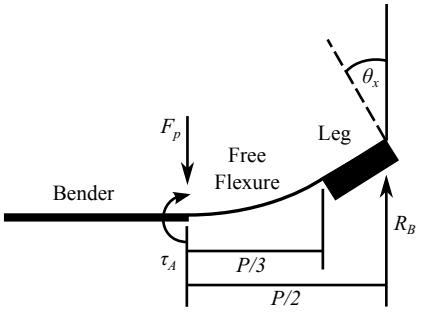

Fig. 6. Boundary conditions for flexure

The rotational inertia of a volume is found by performing the integral $I = \int_V \rho(r)r^2\,\mathrm{d}V$ for the volume, where r is the distance from the axis of rotation to a mass element $\rho(r)\,\mathrm{d}V$. In the case of the end-effector a compact cross

section is assumed, reducing the integral to be evaluated over the length of the end-effector such that,

$$I_{lx} = \int_0^{l_l} \rho_l A(y) y^2 \, \mathrm{d}y. \tag{21}$$

The lumped inertias of the flexure and actuators are found by assuming a concentrated mass at a distance $r = \frac{P}{2}$ from the center of rotation and ignoring the mass of the free flexure (unsupported section of flexure as shown in Fig. 6) such that,

$$I = mr^2, \tag{22}$$

$$I_{fx} = M_f \left(\frac{P}{2}\right)^2, \tag{23}$$

$$I_{px} = M_p \left(\frac{P}{2}\right)^2. \tag{24}$$

C. Rotation DoF θ_z

The lumped mass model for the z-axis rotational DoF can be seen in Fig. 7. The reference axis for this DoF is located through the centroid of the flexure with respect to the x-y plane as shown in Fig. 2. The lumped inertia and rotational stiffness are found using the Rayleigh method described in the y-axis DoF section such that,

$$K_{\theta z} = K_{fz}, \tag{25}$$

$$I_z = (I_{pz} + I_{fz})B^2 + \frac{I_{lz}}{2}, \tag{26}$$

$$B = \frac{K_{fz}}{K_{fz} + K_{pz}}, \tag{27}$$

where $K_{\theta z}$, K_{fz} and K_{pz} are the rotational stiffness with respect to the z-axis model, the flexure and the actuator respectively and I_z, I_{pz} and I_{fz} are the rotational inertias of the equivalent system, actuator and flexure respectively.

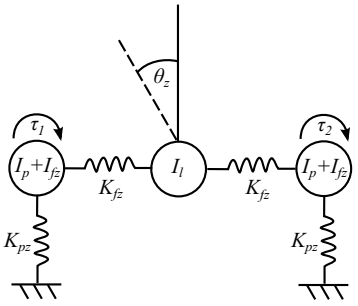

Fig. 7. Lumped mass model for the θ_z DoF

The rotational stiffness for the flexure is found by analyzing the torsional stiffness of the flexure, given by the equation,

$$K = \frac{JG}{l}, \tag{28}$$

$$J_{fz} = \frac{1}{3} w_f t_f^3, \tag{29}$$

$$K_{fz} = \frac{3 G_f J_{fz}}{P}. \tag{30}$$

where K is the flexural stiffness, J is the torsion constant, G is the shear modulus and l is the length.

The rotational stiffness of the piezoelectric bender at the tip can be found using Hooke's law and the equations for motion of the piezoelectric bender from [15] and [17] such that,

$$K_{pz} = \frac{D w_p}{l_p}. \tag{31}$$

The rotational inertia of the flexure is calculated using the integral,

$$I_{fz} = \int_A \rho_f l_f r^2 \, \mathrm{d}A \tag{32}$$

$$= \int_y \int_x \rho_f l_f (x^2 + y^2) \, \mathrm{d}x \mathrm{d}y \tag{33}$$

$$= \frac{m_f (w_f^2 + t_f^2)}{12}, \tag{34}$$

where x and y are measured from the rotational z-axis. The rotational inertia of the leg is identical to that of the x-axis rotational inertia shown in Eq. 21.

The method used to determine rotational inertia of the actuator, I_{pz}, is slightly more complicated due to the loading conditions of the piezoelectric bender. To simplify the calculation the actuator is assumed to have a concentrated cross section such that the integral will only be along the x-axis. To determine I_{pz}, first the angular velocity, $\Omega_p(x)$, and linear momentum, $\mathrm{d}L_p(x)$, must be found with respect to the rotational axis,

$$\mathrm{d}L_p(x) = \rho_p w_p t_p v_p(x)(N - x)\mathrm{d}x, \tag{35}$$

$$\Omega_p(x) = \frac{v_p(x)}{(N - x)}, \tag{36}$$

where $v_p(x)$ is the velocity of the actuator with respect to x and $N = l_p - \frac{w_f}{2}$ is the distance from the base of the actuator to the z reference axis. Using these equations and integrating along the length of the beam, the rotational inertia is,

$$\mathrm{d}I_{pz} = \frac{\mathrm{d}L_p(x)}{\Omega_p(x)} = \rho_p w_p t_p N^2 \left(1 - \frac{x}{N}\right)^2 \mathrm{d}x, \tag{37}$$

$$I_{pz} = \int_0^{l_p} \rho_p w_p t_p N^2 \left(1 - \frac{x}{N}\right)^2 \mathrm{d}x \tag{38}$$

$$= m_p N^2 \left(1 - \frac{L}{N} + \frac{L^2}{3N^2}\right). \tag{39}$$

D. Finite element analysis

The leg was also analyzed using the FEA tool ANSYS to determine the range of motion and resonance modes of the leg. This analysis showed that the first two resonance modes were dominated by rotational motion about the x and z reference axis. The first two resonant modes can be seen in Fig. 8. The third resonance was significantly higher that the first two and features significant displacement along the y-axis, corresponding to the δ_y DoF.

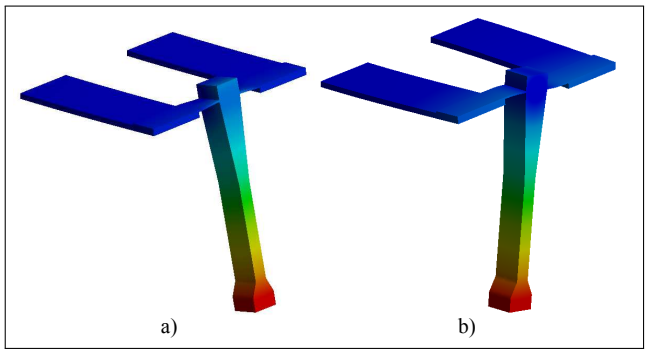

Fig. 8. a) First resonant mode shape, b) Second resonant mode shape

E. Discussions

By analyzing the equations for stiffness, mass and inertia, insights into the parameters that effect the resonant frequencies can be determined.

This work has highlighted several parameters that have a significant effect over particular modes compared to others. The length of the bender has a moderate impact on the δ_y resonant frequency and a significant effect on the resonant frequency for the θ_x mode while having very little effect on the θ_z resonance. This feature can be exploited to change the θ_x resonant frequency with a marginal alteration to the free length of the actuators. Conversely the separation distance P has a minimal effect on the θ_x mode but a significant impact on the δ_y and θ_z modes. Care must be taken when tuning the resonant frequencies using these two methods to not affect the stiffness and therefore the maximum displacements.

An alternative method of tunning the resonant frequencies is to alter the lumped masses of the leg. If done correctly, adding or removing masses will have little to no effect on the stiffness and therefore maximum displacements of the beam. The simplest method of tuning the mass of the leg is to change the shape of the end effector. Increasing mass at the base of the leg will have a minimal impact on the rotational DoFs as this mass is located very near to the axis of rotation. Conversely, mass added or removed from the tip will significantly alter the resonant frequencies of the rotational DoFs.

IV. Experimental Results

An experimental analysis was conducted using a prototype leg identical in design to the leg shown in Fig. 2 and Fig. 9. The purpose of this analysis was to determine the frequency responses and the static displacements of the leg so as to verify the analytical model. The control signals for the piezoelectric benders were generated using an Agilent 33500B dual channel signal generator connected to two Pdm200 voltage amplifier from PiezoDrive to generate the high voltage driving signals. The leg end effector velocities were measured using a PDV 100 laser vibrometer from Polytec and the low frequency displacements were measured with an LAT61 laser distance sensor from disoric.

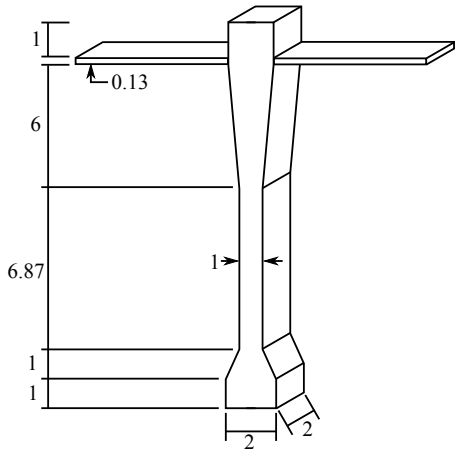

Fig. 9. Miniature robot leg end effector. All dimensions are in mm

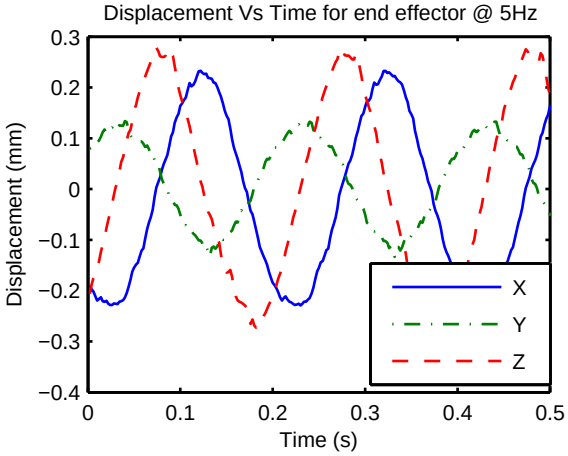

Fig. 10. Experimental end-effector displacement with actuators driven 90° out of phase at 5 Hz.

The leg was constructed using two custom made piezoelectric benders measuring 4.5 mm wide, 0.4 mm thick by 15 mm in length. The actuators were glued to a 3-D printed, ABS plastic base 6 mm apart with two part epoxy and with a free length of approximately 12.8 mm. The leg end effector and flexure was machined out of a single piece of aluminum and glued across the tips of the actuators.

The end effector x, y and z axis displacements were measured by driving the benders 90° out of phase at a frequency of 5 Hz. All displacement measurements were taken at the tip of the end-effector. The displacements achieved were 462.2 μm in the x-axis, 250.1 μm in the y-axis and 552.1 μm in the z-axis as shown in Fig. 10.

The frequency response shown in Fig. 11, identifies resonances at approximately 270 Hz, 360 Hz and 720 Hz for the x, z and y axis respectively. This response was generated by driving both benders with identical noise with a peak to peak voltage of 10 V and a bandwidth of 1 kHz. This result compares reasonably well with both the FEA and analytical analysis shown in Table. I. The coupling shown in Fig. 11 between the different axis is

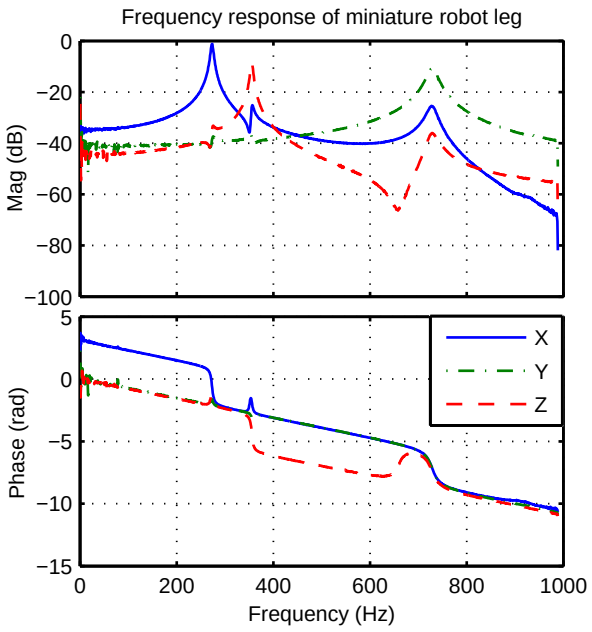

Fig. 11. Frequency response of miniature robotic leg in x, y and z axis.

primarily due to the alignment of the vibrometer with respect to the leg, and the alignment of the components of the leg during the assembly process.

Discrepancies between the experimental, FEA and analytical results are contributed to the imperfect mounting and assembly of the leg structure and the non-rigid nature of the support structure, overall resulting in a less stiff structure. Damping is also present in the real world results and the lumped mass model ignores twisting and shear stress of the piezoelectric actuators. Lastly, the analytical and FEA models do no account for any non-linear effects due to the piezoelectric actuators.

V. Conclusion

The experimental results show that a miniature robotic leg produced in this way can provide enough force and motion to achieve significant motion of the end-effector. The main shortcomings of this design is the repeatability of the leg construction. In order to improve this the manufacturing process must be simplified to attain a uniform and repeatable leg. Another approach to this problem is to fine tune the resonant modes after construction such that the resonant frequencies of all the robots legs are equal. Ideally a combination of these improvements will be investigated

TABLE I

First resonant modes for each DoF

DoF	Lumped Mass	FEA	Experimental
δ_y	1030	946 Hz	720 Hz
θ_x	391 Hz	427 Hz	360 Hz
θ_z	334 Hz	410 Hz	270 Hz

The next step will be to analyze the response of the leg during intermittent ground contact. Preliminary results have shown that an intermittent ground contact will have a damping effect of the frequency response of the leg, however this is greatly dependent on a wide range of variables and more research is required. The final goal of this research is to develop an untethered, autonomous hexapod miniature robot.

References

[1] C. Zhu, "In-pipe robot for inspection and sampling tasks," *Industrial Robot: An International Journal*, vol. 34, no. 1, pp. 39–45, 2007.

[2] J. Casper and R. R. Murphy, "Human-robot interactions during the robot-assisted urban search and rescue response at the World Trade Center." *IEEE transactions on systems, man, and cybernetics. Part B, Cybernetics : a publication of the IEEE Systems, Man, and Cybernetics Society*, vol. 33, no. 3, pp. 367–85, Jan. 2003.

[3] L. Zhang, Q. Huang, Y. Li, J. Gao, H. Li, and L. Wu, "Research and development of throwable miniature reconnaissance robot," *2012 IEEE International Conference on Mechatronics and Automation*, pp. 1254–1259, Aug. 2012.

[4] O. Dolghi, K. W. Strabala, T. D. Wortman, M. R. Goede, S. M. Farritor, and D. Oleynikov, "Miniature in vivo robot for laparoendoscopic single-site surgery." *Surgical endoscopy*, vol. 25, no. 10, pp. 3453–8, Oct. 2011.

[5] J. Paradiso and T. Starner, "Energy scavenging for mobile and wireless electronics," *Pervasive Computing, IEEE*, 2005.

[6] D. Chen, J. Yin, K. Zhao, W. Zheng, and T. Wang, "Bionic Mechanism and Kinematics Analysis of Hopping Robot Inspired by Locust Jumping," *Journal of Bionic Engineering*, vol. 8, no. 4, pp. 429–439, 2011.

[7] R. Sahai, S. Avadhanula, R. Groff, E. Steltz, R. Wood, and R. S. Fearing, "Towards a 3g crawling robot through the integration of microrobot technologies," in *Robotics and Automation, 2006. ICRA 2006. Proceedings 2006 IEEE International Conference on.* IEEE, 2006, pp. 296–302.

[8] N. Roy, P. Newman, and S. Srinivasa, "Multi-Stage Micro Rockets for Robotic Insects," *Robotics*, p. 185, 2013.

[9] A. T. Baisch, P. S. Sreetharan, and R. J. Wood, "Biologically-Inspired Locomotion of a 2g Hexapod Robot," *International Conference on Intelligent Robots and Systems*, pp. 5360–5365, 2010.

[10] J. P. Whitney and R. J. Wood, "Conceptual design of flapping-wing micro air vehicles." *Bioinspiration & biomimetics*, vol. 7, no. 3, p. 036001, Sep. 2012.

[11] K. Y. Ma, P. Chirarattananon, S. B. Fuller, and R. J. Wood, "Controlled flight of a biologically inspired, insect-scale robot." *Science (New York, N.Y.)*, vol. 340, no. 6132, pp. 603–7, May 2013.

[12] A. T. Baisch, C. Heimlich, M. Karpelson, and R. J. Wood, "HAMR 3 : An Autonomous 1 . 7g Ambulatory Robot," pp. 5073–5079, 2011.

[13] F. Becker, K. Zimmermann, V. T. Minchenya, and T. Volkova, "Piezo-driven Micro Robots for Different Environments : Prototypes and Experiments," pp. 41–45, 2012.

[14] D. M. Aukes and R. J. Wood, "Monolithic Design and Fabrication of a 2-DOF Bio-Inspired Leg Transmission," pp. 1–10, 2014.

[15] S. A. Rios and A. J. Fleming, "A Novel Electrical Configuration for Three Wire Piezoelectric Bimorph," 2014.

[16] W. C. Young and R. G. Budynas, *Roarks Formulas for Stress and Strain*, 7th ed. McGraw-Hill Companies, The, 2002.

[17] Q. M. Wang and L. E. Cross, "Constitutive equations of symmetrical triple layer piezoelectric benders." *IEEE transactions on ultrasonics, ferroelectrics, and frequency control*, vol. 46, no. 6, pp. 1343–51, Jan. 1999.